Supporting Information

Tunable Exchange Bias in Hofmann MOF-Derived α-Fe_2O_3/Pt magnetic composites

Su-Yun Zhang[a], Zhu Ding[b], Zihao Wang[a], Junzhe Tao[a], Yu-Jia Zeng[a,*]

[a] Key Laboratory of Optoelectronic Devices and Systems of Ministry of Education and Guangdong Province, College of Physics and Optoelectronic Engineering, Shenzhen University, Shenzhen, 518060, P. R. China

E-mail: yjzeng@szu.edu.cn

[b] Faculty of Mathematics and Physics, Huaiyin Institute of Technology, Huaian, 223003, P. R. China

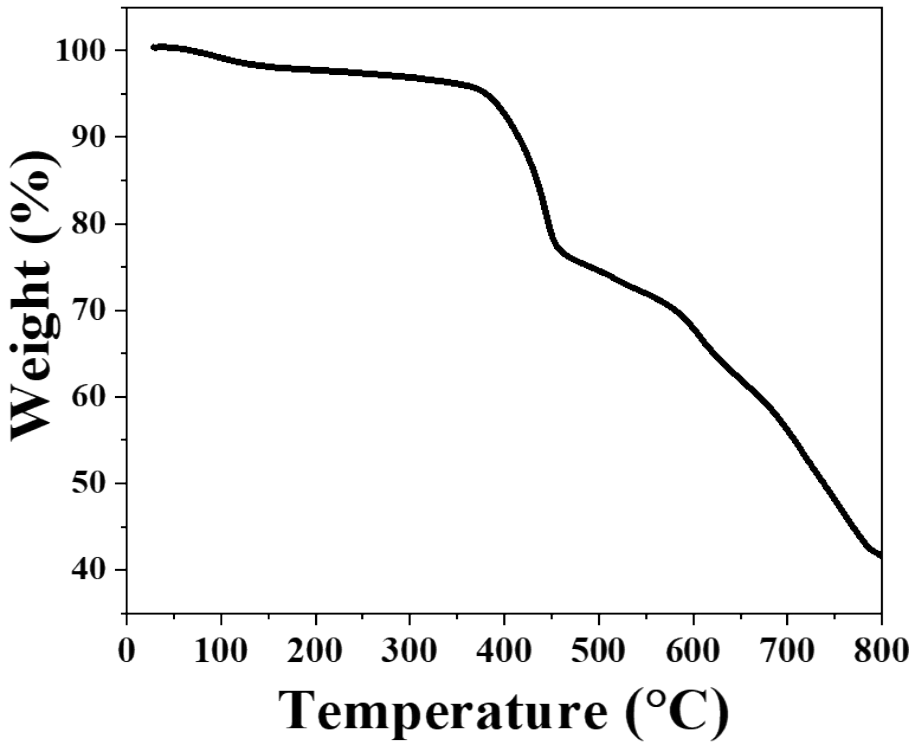

Figure S1. TGA curve of Hofmann-type Pt/Fe-MOF.

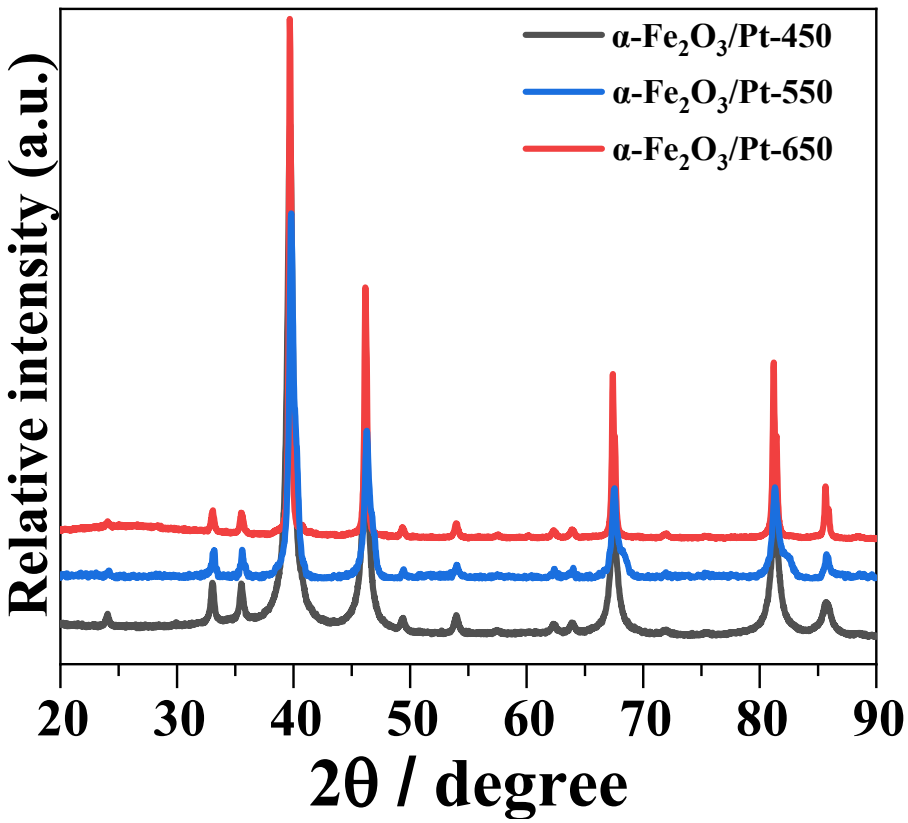

Figure S2. Powder XRD patterns of α-Fe_2O_3/Pt composites derived from a Hofmann-type Pt/Fe-MOF at 450, 550, and 650 °C.

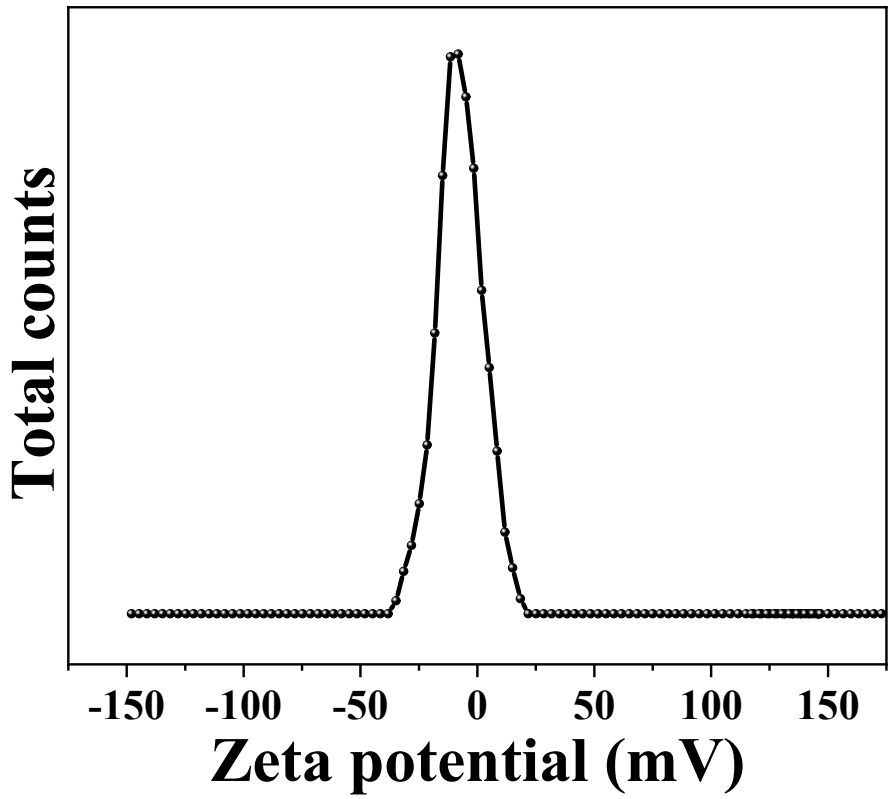

Figure S3. Zeta potential of Hofmann-type Pt/Fe-MOF.

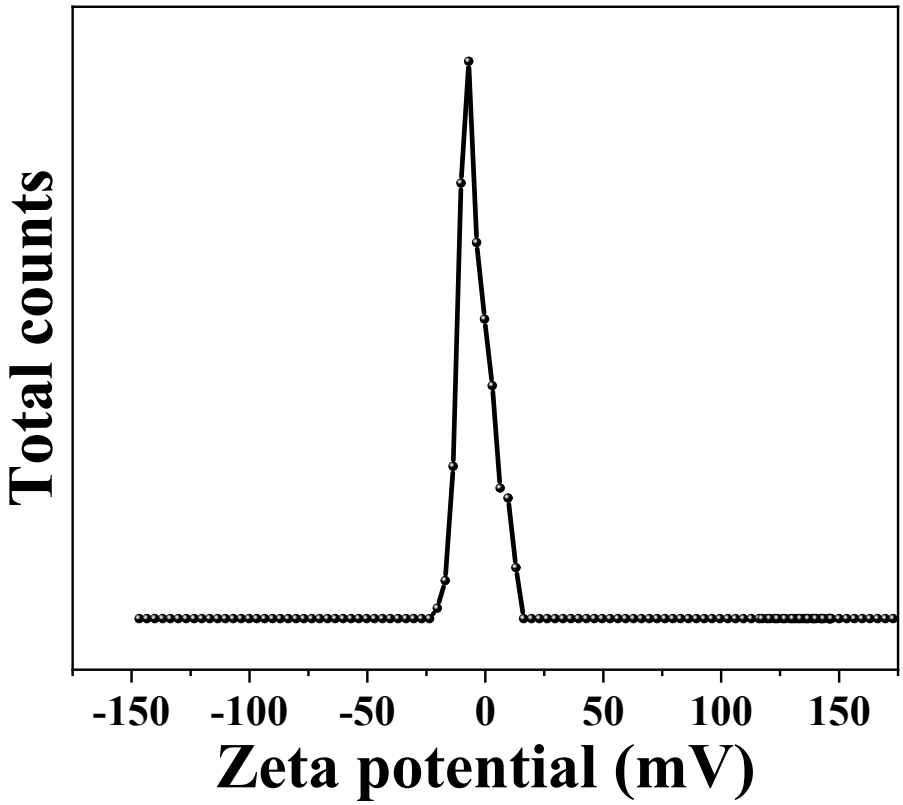

Figure S4. Zeta potential of α-Fe_2O_3/Pt-450.

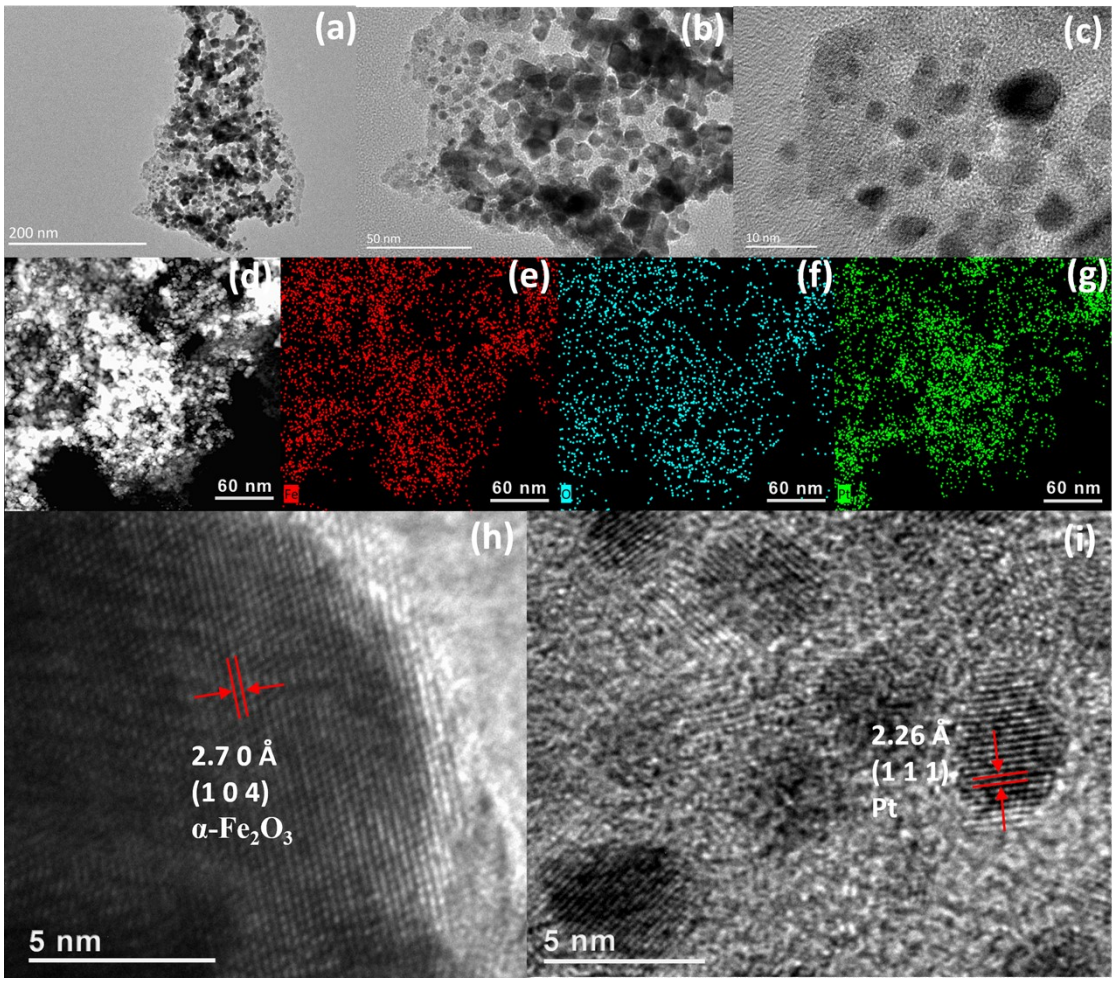

Figure S5. Microstructural and compositional analysis of α-Fe_2O_3/Pt-550. (a-c) TEM images revealing the overall morphology. (d-g) EDS elemental maps illustrating the homogeneous distribution of Fe (red) and O (cyan), with Pt nanoparticles (green) well-dispersed on the support. (h, i) HRTEM images identifying the crystalline structures of both α-Fe_2O_3 and Pt.

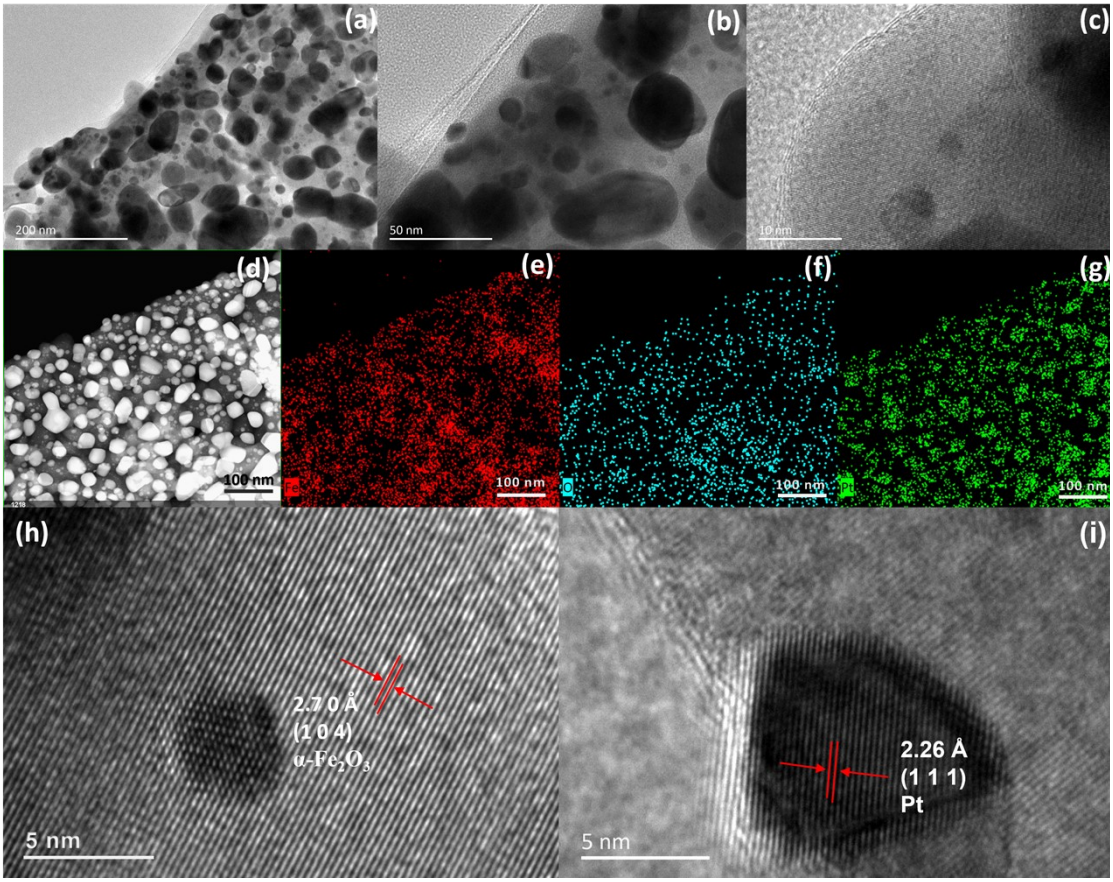

Figure S6. Microstructural and compositional analysis of α-Fe_2O_3/Pt-650. (a-c) TEM images revealing the overall morphology. (d-g) EDS elemental maps illustrating the homogeneous distribution of Fe (red) and O (cyan), with Pt nanoparticles (green) well-dispersed on the support. (h, i) HRTEM images identifying the crystalline structures of both α-Fe_2O_3 and Pt.

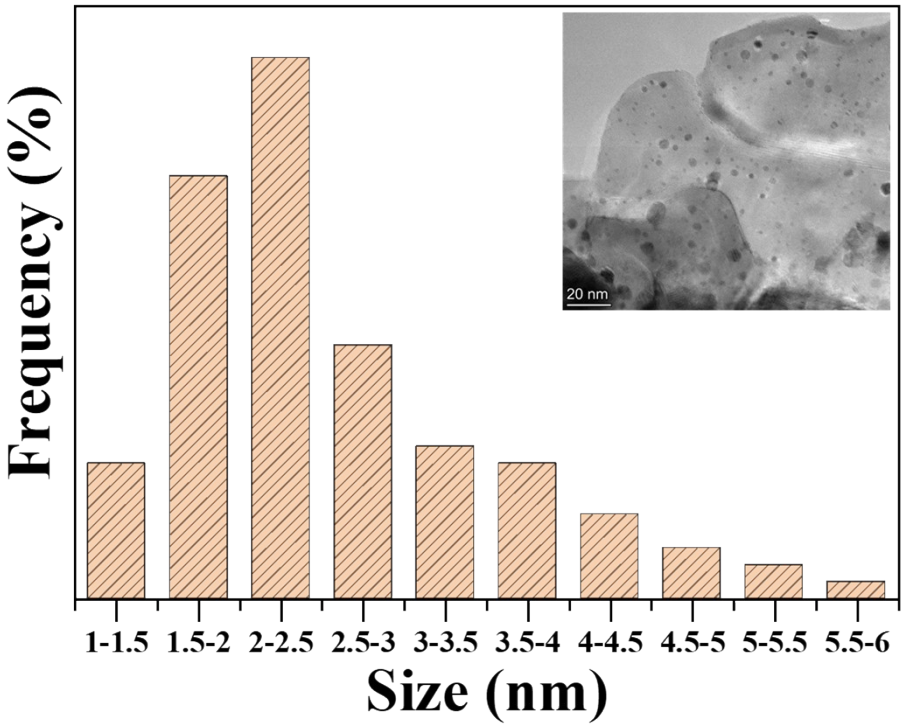

Figure S7. Particle size distribution of Pt for sample α-Fe_2O_3/Pt-450.

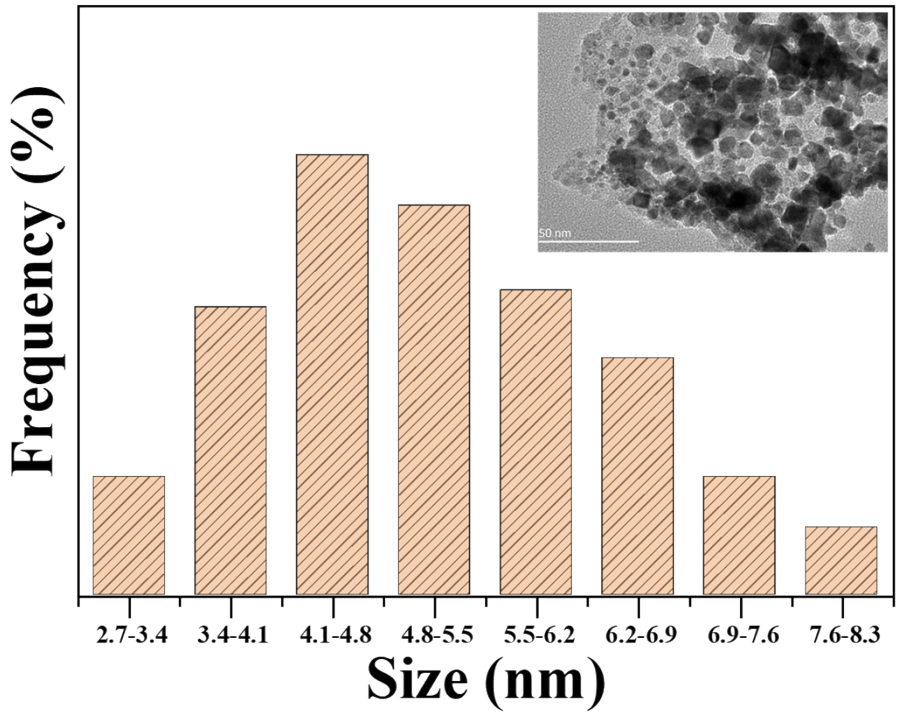

Figure S8. Particle size distribution of Pt for sample α-Fe_2O_3/Pt-550.

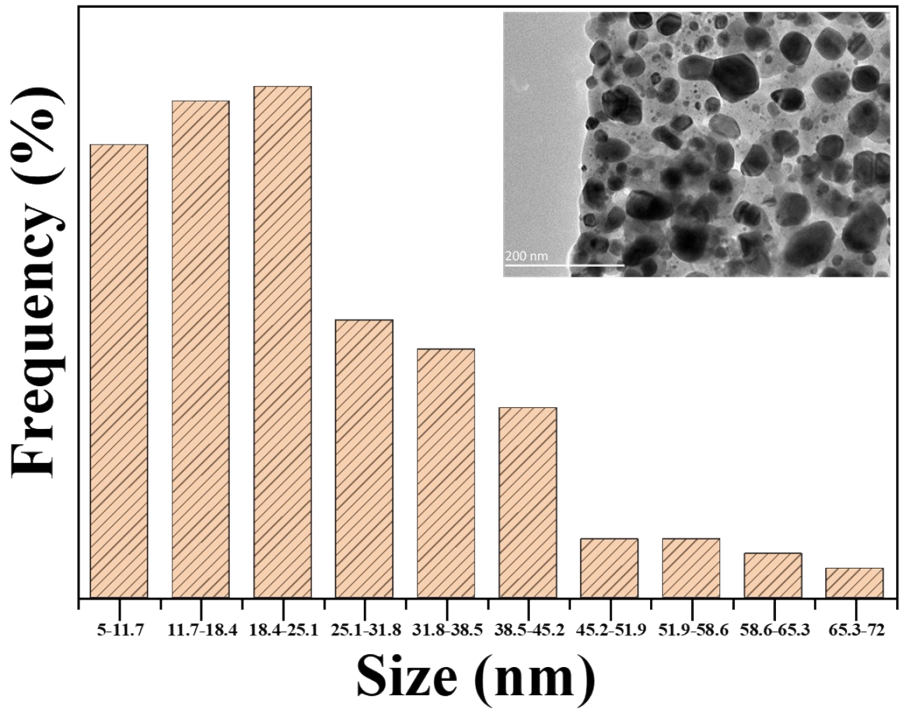

Figure S9. Particle size distribution of Pt for sample α-Fe_2O_3/Pt-650.

Table S1. The H_C of α-Fe_2O_3/Pt-450, α-Fe_2O_3/Pt-550, and α-Fe_2O_3/Pt-650 at different temperatures. It was evaluated by $|H_c| = |(H_1-H_2)/2|$, where H_1, H_2 is the left intercept and right intercept of the X-axis of the hysteresis line at M = 0.

T / sample	2 K	100 K	200 K	300 K	350 K
α-Fe_2O_3/Pt-450	1177	83.5	16	14.5	5.5
α-Fe_2O_3/Pt-550	1174	332	166	178.5	153
α-Fe_2O_3/Pt-650	689.5	257	432	1806.5	1632

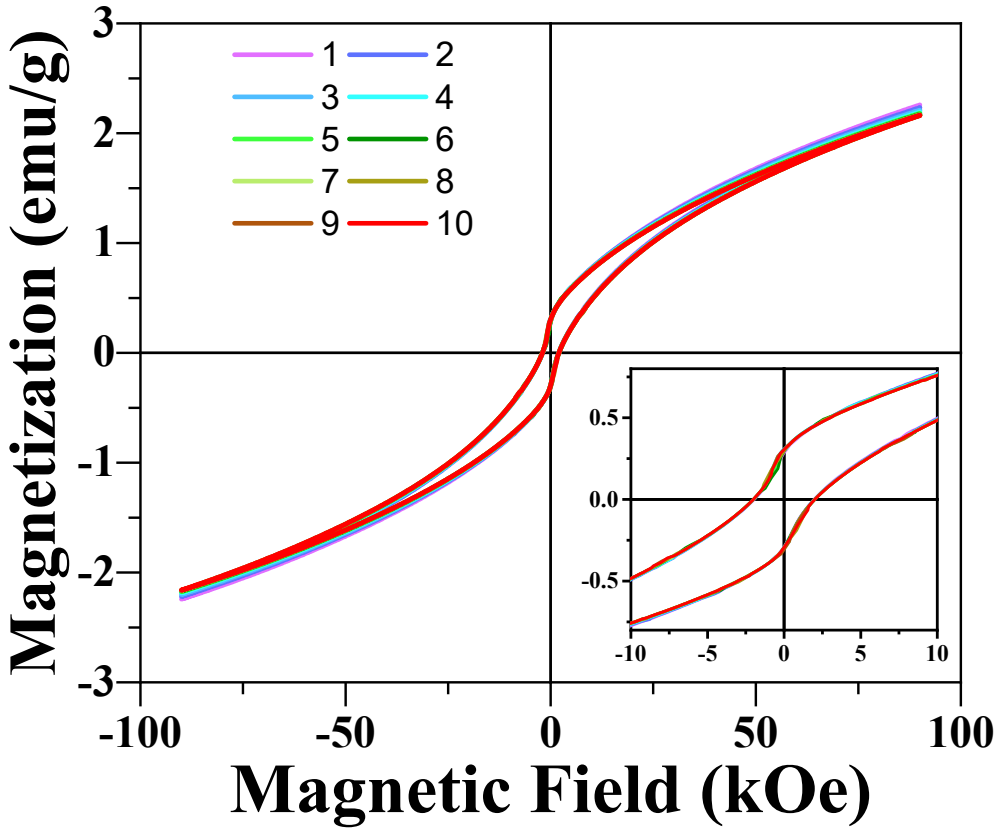

Figure S10. Magnetic hysteresis loops of 10 cycles measured at 5 K under zero-field-cooling of α-Fe_2O_3/Pt-450.

Table S2. M-H parameters of α-Fe_2O_3/Pt-450, α-Fe_2O_3/Pt-550, and α-Fe_2O_3/Pt-650 at 2 K, 30 K, 60 K and 100 K under a cooling field of 40 kOe. H_1, H_2: The left intercept and right intercept of the X-axis of the hysteresis line at M = 0. $|H_c| = |(H_1-H_2)/2|$ and $|H_{EB}| = |(H_1+H_2)/2|$.

	H_1 (Oe)	**H_2 (Oe)**	**H_c (Oe)**	**H_{EB} (Oe)**
Sample	2 K			
α-Fe_2O_3/Pt-450	-4838	640	2,739	2,099
α-Fe_2O_3/Pt-550	-2369	930	1649.5	719.5
α-Fe_2O_3/Pt-650	-972	321	646.5	325.5
	30 K			
α-Fe_2O_3/Pt-450	-610	520	565	45
α-Fe_2O_3/Pt-550	-594	468	531	63
α-Fe_2O_3/Pt-650	-477	126	301.5	175.5
	60 K			
α-Fe_2O_3/Pt-450	-192	175	183.5	8.5
α-Fe_2O_3/Pt-550	-258	181	219.5	38.5
α-Fe_2O_3/Pt-650	-430	73	251.5	178.5
	100 K			
α-Fe_2O_3/Pt-450	-90	75	82.5	7.5
α-Fe_2O_3/Pt-550	-105	65	85	20
α-Fe_2O_3/Pt-650	-455	58	256.5	198.5

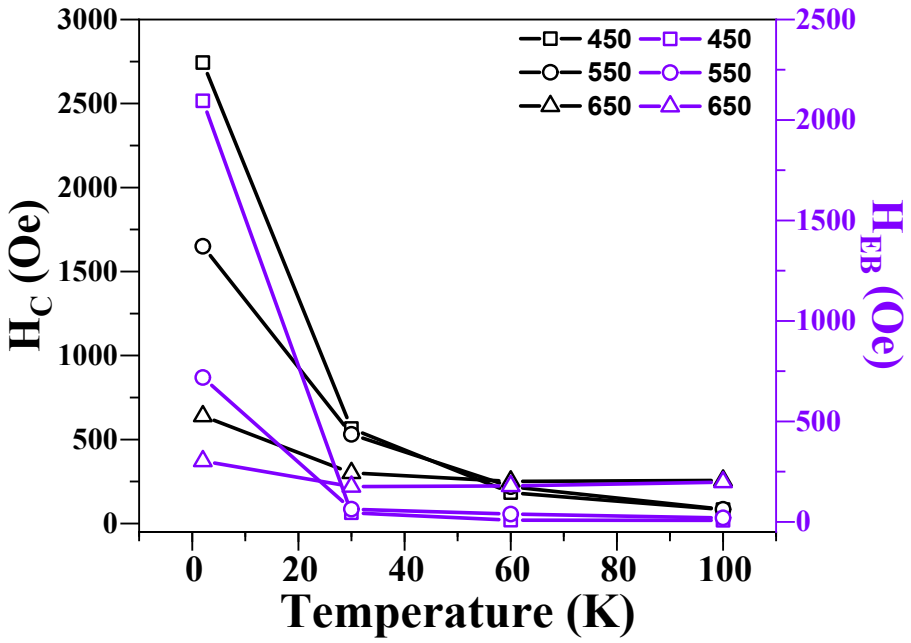

Figure S11. The coercivity H_C (black) and exchange bias H_{EB} (purple) of α-Fe_2O_3/Pt-450, α-Fe_2O_3/Pt-550, and α-Fe_2O_3/Pt-650 under a cooling field of 40 kOe at different temperatures.

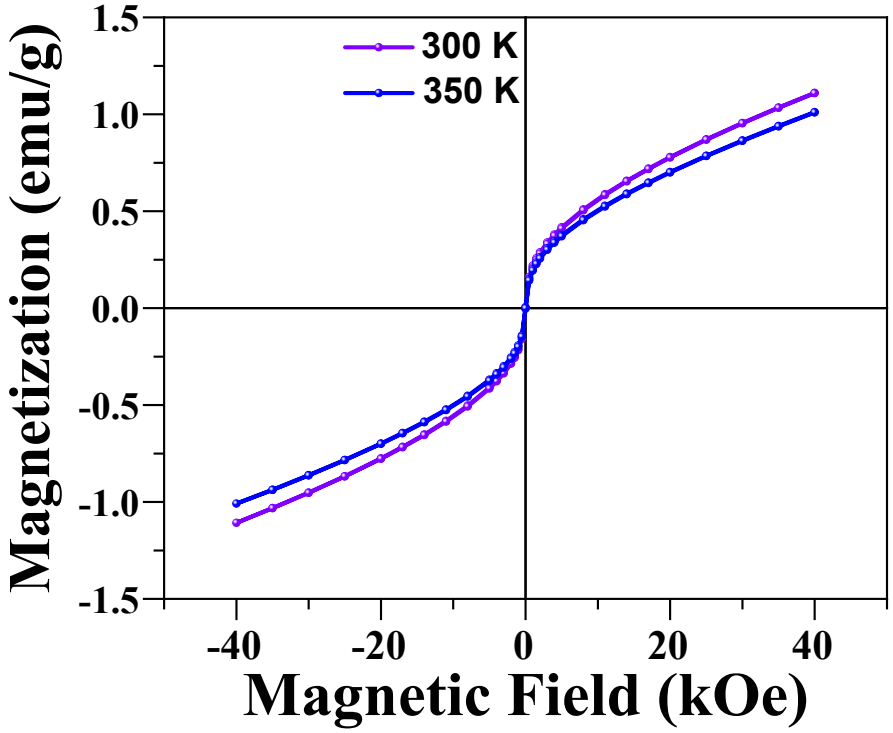

Figure S12. Magnetic hysteresis loops of α-Fe_2O_3/Pt-450 at 300 and 350 K under a cooling field of 60 kOe.

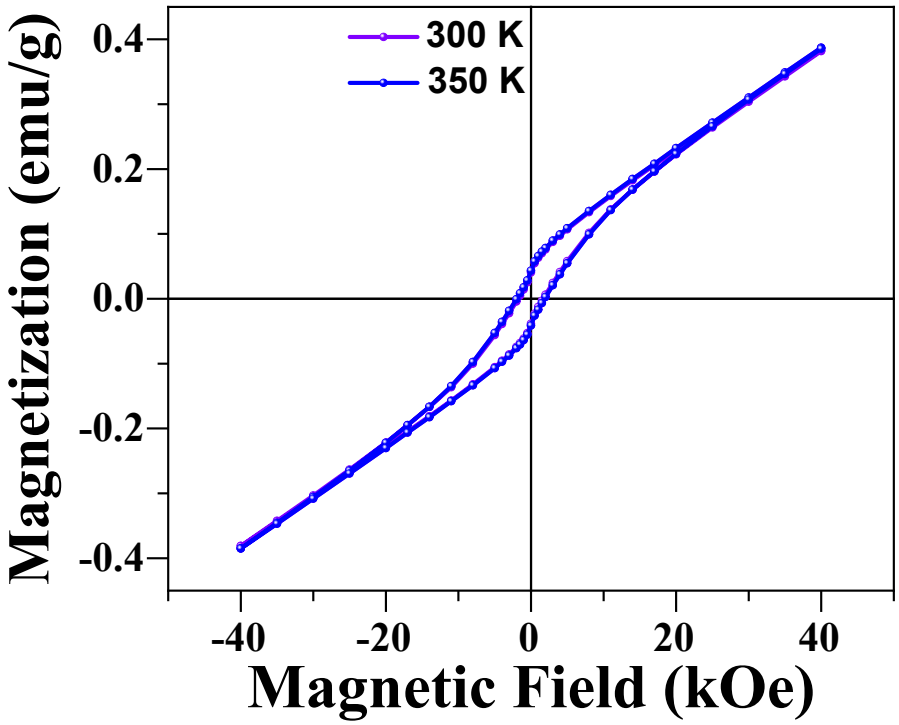

Figure S13. Magnetic hysteresis loops of α-Fe_2O_3/Pt-650 at 300 and 350 K under a cooling field of 60 kOe.

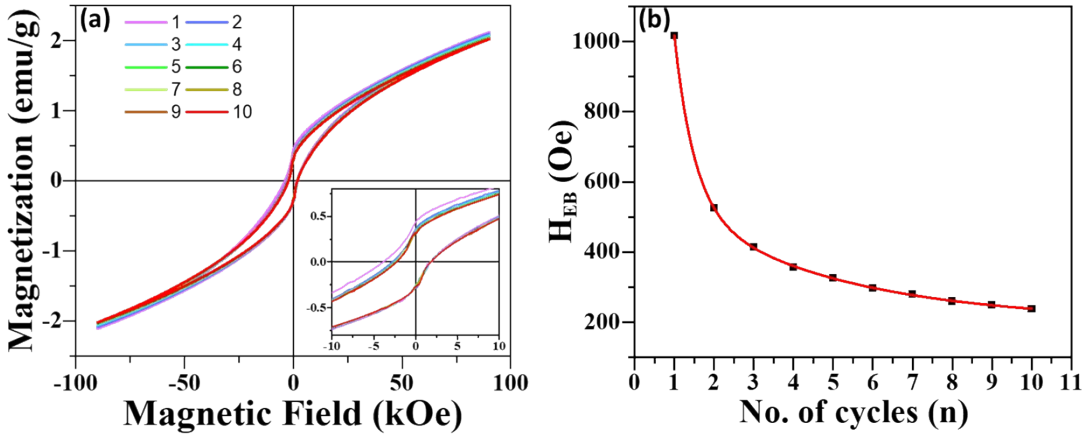

Figure S14. (a) Training effect in α-Fe_2O_3/Pt-450: consecutive hysteresis loops measured at 5 K after field cooling under 60 kOe. (b) The fit data according to the power law.

Table S3. The H_C and H_{EB} value of α-Fe_2O_3/Pt-450 for 10 cycles measured at 5 K under a cooling field of 60 kOe. $|H_c| = |(H_1-H_2)/2|$ and $|H_{EB}| = |(H_1+H_2)/2|$, where H_1, H_2 is the left intercept and right intercept of the X-axis of the hysteresis line at M = 0.

n	**1**	**2**	**3**	**4**	**5**	**6**	**7**	**8**	**9**	**10**
H_C	2860	2278	2148	2134	2117	2088.5	2074	2063.5	2049	2037.5
H_{EB}	1017	525	414	357	326	296.5	280	259.5	249	237.5

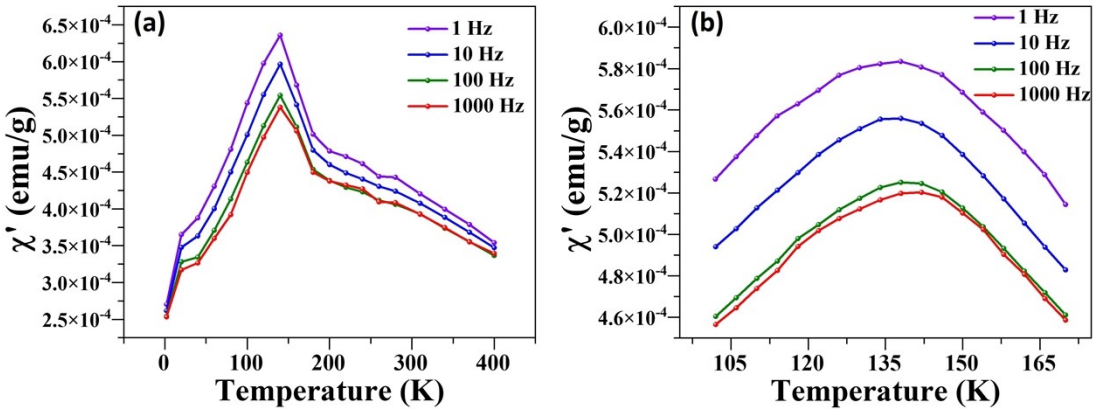

Figure S15. (a) AC susceptibilities of α-Fe_2O_3/Pt-450 at different frequencies. (b) The detailed measurement near the phase transition point.

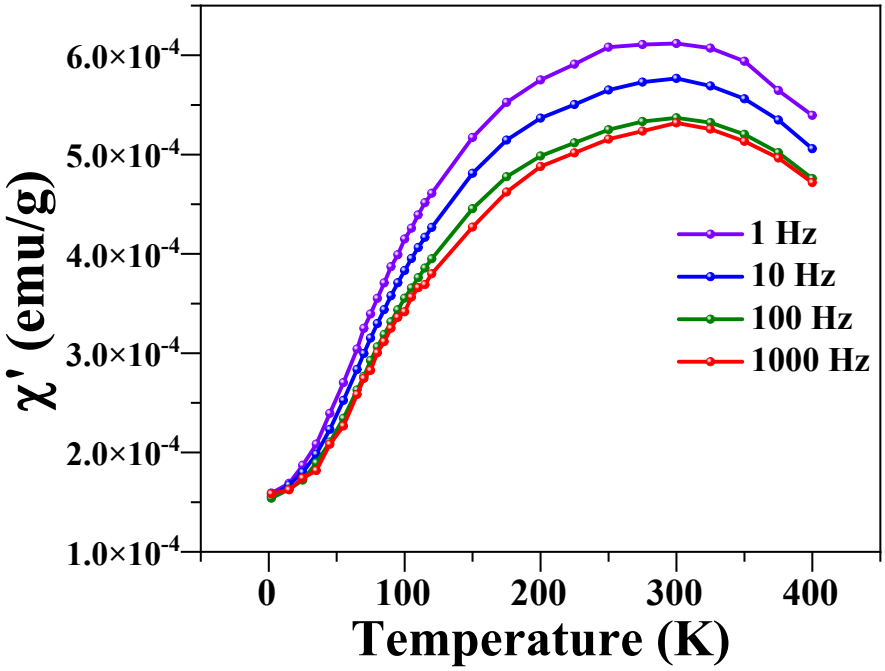

Figure S16. AC susceptibilities of α-Fe_2O_3/Pt-550 at different frequencies.

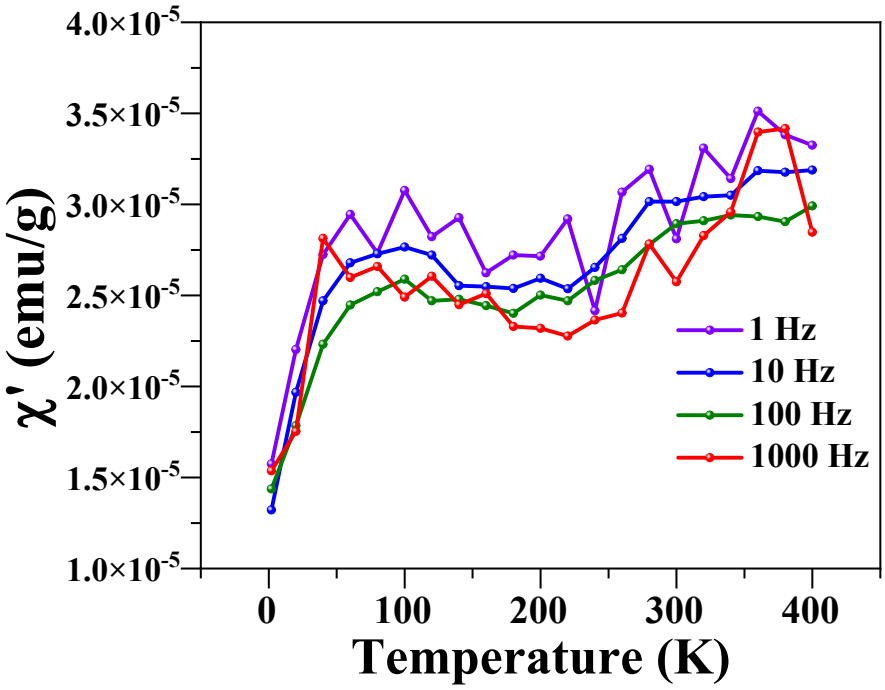

Figure S17. AC susceptibilities of α-Fe_2O_3/Pt-650 at different frequencies.

Table S4. M-H parameters of α-Fe_2O_3/Pt-450, α-Fe_2O_3/Pt-550, and α-Fe_2O_3/Pt-650 at 2 K under different cooling fields. H_1, H_2: The left intercept and right intercept of the X-axis of the hysteresis line at M = 0. $|H_c| = |(H_1-H_2)/2|$ and $|H_{EB}| = |(H_1+H_2)/2|$.

	H_1 (Oe)	H_2 (Oe)	H_c (Oe)	H_{EB} (Oe)
Sample	10 kOe			
α-Fe_2O_3/Pt-450	-3869	446	2157.5	1711.5
α-Fe_2O_3/Pt-550	-2245	1008	1626.5	618.5
α-Fe_2O_3/Pt-650	-972	321	646.5	325.5
	20 kOe			
α-Fe_2O_3/Pt-450	-4791	474	2632.5	2158.5
α-Fe_2O_3/Pt-550	-2358	874	1616	742
α-Fe_2O_3/Pt-650	-972	321	646.5	325.5
	40 kOe			
α-Fe_2O_3/Pt-450	-4838	640	2,739	2,099
α-Fe_2O_3/Pt-550	-2369	930	1649.5	719.5
α-Fe_2O_3/Pt-650	-972	321	646.5	325.5
	60 kOe			
α-Fe_2O_3/Pt-450	-6049	511	3,280	2,769
α-Fe_2O_3/Pt-550	-2334	970	1652	682
α-Fe_2O_3/Pt-650	-972	321	646.5	325.5

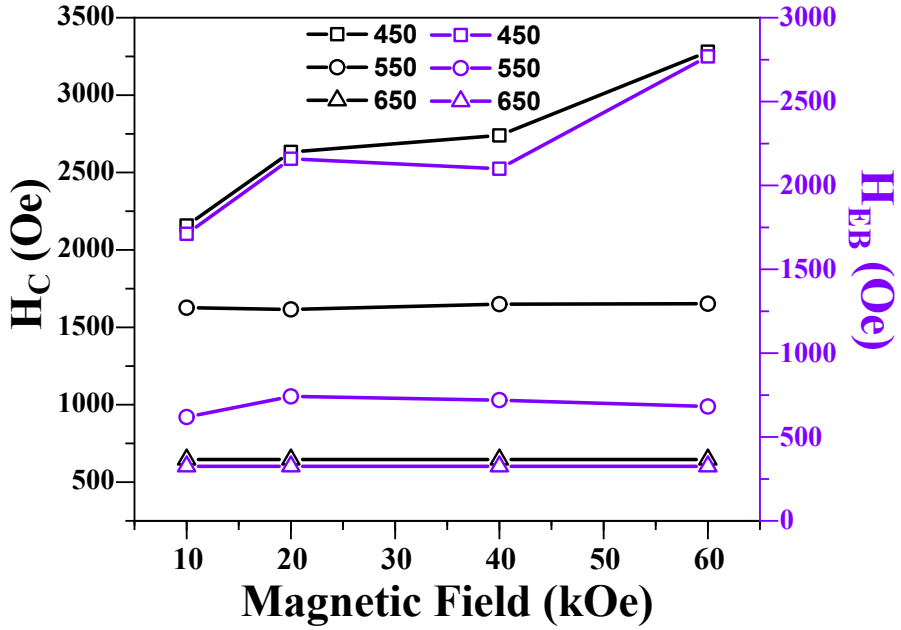

Figure S18. The coercivity H_C (black) and exchange bias H_{EB} (purple) of α-Fe_2O_3/Pt-450, α-Fe_2O_3/Pt-550, and α-Fe_2O_3/Pt-650 at 2 K under different cooling fields.